Journal of Medicinal Chemistry

Article

A Fragment-Based Approach to the Development of an Orally Bioavailable Lactam Inhibitor of Lipoprotein-Associated Phospholipase A2 (Lp-PLA)

Alison J.-A. Woolford, Philip J. Day, Véronique Bénéton, Valerio Berdini, Joseph E. Coyle, Yann Dudit, Pascal Grondin, Pascal Huet, Lydia Y. W. Lee, Eric S. Manas, Rachel L. McMenamin, Christopher W Murray, Lee W. Page, Vipulkumar K. Patel, Florent Potvain, Sharna J. Rich, Yingxia Sang, Don O. Somers, Lionel Trottet, Zehong Wan, and Xiaomin Zhang

J. Med. Chem., **Just Accepted Manuscript** • DOI: 10.1021/acs.jmedchem.6b01427 • Publication Date (Web): 10 Nov 2016

A Fragment-Based Approach to the Development of an Orally Bioavailable Lactam Inhibitor of Lipoprotein-Associated Phospholipase A2 (Lp-PLA$_2$)

Alison J.-A. Woolford,*[,†,#] Philip J. Day,[†,#] Véronique Bénéton,[‖] Valerio Berdini,[†] Joseph E. Coyle,[†] Yann Dudit,[‖] Pascal Grondin,[‖] Pascal Huet,[‖] Lydia Y. W. Lee,[†] Eric S. Manas,[§] Rachel L. McMenamin,[†] Christopher W. Murray,[†] Lee W. Page,[†] Vipulkumar K. Patel,*[,‡] Florent Potvain,[‖] Sharna J. Rich,[†] Yingxia Sang,[⊥] Don O. Somers,[‡] Lionel Trottet,[‖] Zehong Wan,[⊥] and Xiaomin Zhang.[⊥]

[†]Astex Pharmaceuticals, 436 Cambridge Science Park, Milton Road, Cambridge CB4 0QA, United Kingdom.

[‡]GlaxoSmithKline, Gunnels Wood Road, Stevenage SG1 2NY, United Kingdom.

[§]GlaxoSmithKline, 1250 South Collegeville Road, Collegeville, Pennsylvania 19426, United States.

[‖]Centre de Recherches Francois Hyafil, GlaxoSmithKline, 25–27 Avenue du Québec, Les Ulis, France.

[⊥]Neurodegeneration DPU, GlaxoSmithKline, 898 Halei Road, Zhangjiang Hi-Tech Park, Pudong, Shanghai 201203, China.

ABSTRACT: Lp-PLA$_2$ has been explored as a target for a number of inflammation associated diseases, including cardiovascular disease and dementia. This article describes the discovery of a new fragment derived chemotype that interacts with the active site of Lp-PLA$_2$. The starting fragment hit was discovered through an X-ray fragment screen and

showed no activity in the bioassay (IC_{50} >1mM). The fragment hit was optimised using a variety of structure-based drug design techniques, including virtual screening, fragment merging and improvement of shape complementarity. A novel series of Lp-PLA_2 inhibitors was generated with low lipophilicity and a promising pharmacokinetic profile.

KEYWORDS: Lp-PLA_2, fragment-based drug discovery, structure guided optimisation.

INTRODUCTION

Lp-PLA_2 is a member of the phospholipase A2 superfamily, which specifically cleave the *sn*-2 ester bond of glycerophospholipids.[1] Lp-PLA_2 is found in the plasma and circulates in complex to high and low density lipoproteins.[2] The biological substrate(s) for this lipase are unknown but studies examining hydrolysis of a variety of *sn*-2 acyl chain lengths have shown that Lp-PLA_2 hydrolyses oxidized and truncated phospholipids.[3] Cleavage of oxidatively damaged phospholipid substrates releases pro-inflammatory factors such as lysophosphatidylcholine and oxidized non-esterified fatty acids,[4] which can lead to inflammation in the arteries and cardiovascular disease (CVD).[5] Thus, Lp-PLA_2 is a pro-inflammatory, lipid-modifying, enzyme. The plasma levels of Lp-PLA_2 have been shown to correlate with CVD and Lp-PLA_2 is now an established biomarker. Other diseases that have elevated levels of Lp-PLA_2 include dementia,[6] diabetic macular edema[7] and prostate cancer.[8]

Inhibitors of Lp-PLA_2 have been investigated in the clinic for atherosclerosis[9] and Alzheimer's disease.[10] For example, darapladib (**1**) is an orally bioavailable and very potent inhibitor of Lp-PLA_2 with IC_{50} = 49 pM in a biochemical assay.[11] A secondary 'plasma' assay measures inhibition in whole plasma, which approximates the physiological environment of the enzyme, and darapladib has an IC_{50} = 35 nM.[12-13] Darapladib has

undergone two phase three trials for cardiovascular disease but has been discontinued because it did not meet the primary end points. Several other classes of inhibitors have been reported in the literature but none have yet progressed to the clinic.[14]

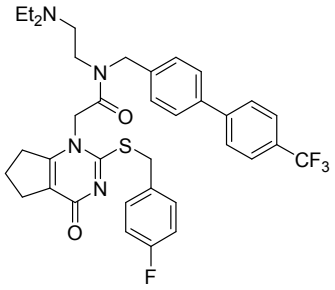

Darapladib (**1**)

The crystal structure of apo Lp-PLA$_2$,[15] and its complex with darapladib,[16] have previously been reported. Lp-PLA$_2$ exhibits the classic lipase α/β-hydrolase fold with a catalytic triad comprised of Ser273, His351 and Asp296 adjacent to an oxyanion hole formed by the backbone NH's of both Leu153 and Phe274. A water molecule occupies the oxyanion hole in apo Lp-PLA$_2$ but is displaced by the pyrimidone carbonyl of darapladib which forms the same two H-bonds to Leu153 and Phe274 (Figure 1a). The bi-aryl rings in darapladib stack upon the fluorophenyl in a hydrophobic collapse and together they fill the lipophilic groove marked by the residues Phe110 and Phe357.[16] The (2-aminoethyl)diethylamine moiety is mainly solvent exposed and is important for the solubility and pharmacokinetic properties of the molecule.[17]

(**a**) (**b**)

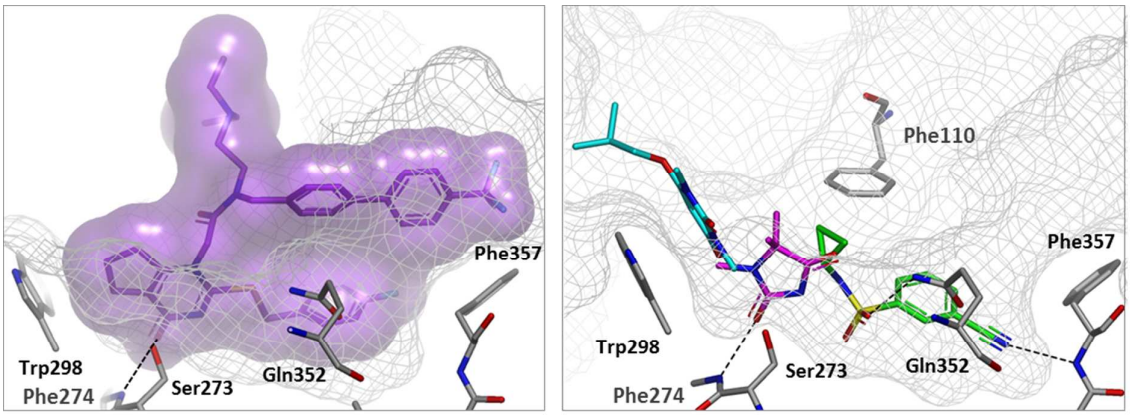

Figure 1. (**a**) X-ray crystal structure darapladib (**1**) bound to Lp-PLA$_2$. The Connolly surface of darapladib is shown in solid purple and the protein as a gray mesh. (**b**) Superposition of the X-ray crystal structures of uracil **2** (cyan), hydantoin **3** (magenta) and sulfonamide **4** (green) bound to Lp-PLA$_2$. Selected residues are shown for clarity. The hydrogen bond interactions are shown as dotted lines.

(**a**) Uracil **2** (**b**) Hydantoin **3** (**c**) Sulfonamide **4**

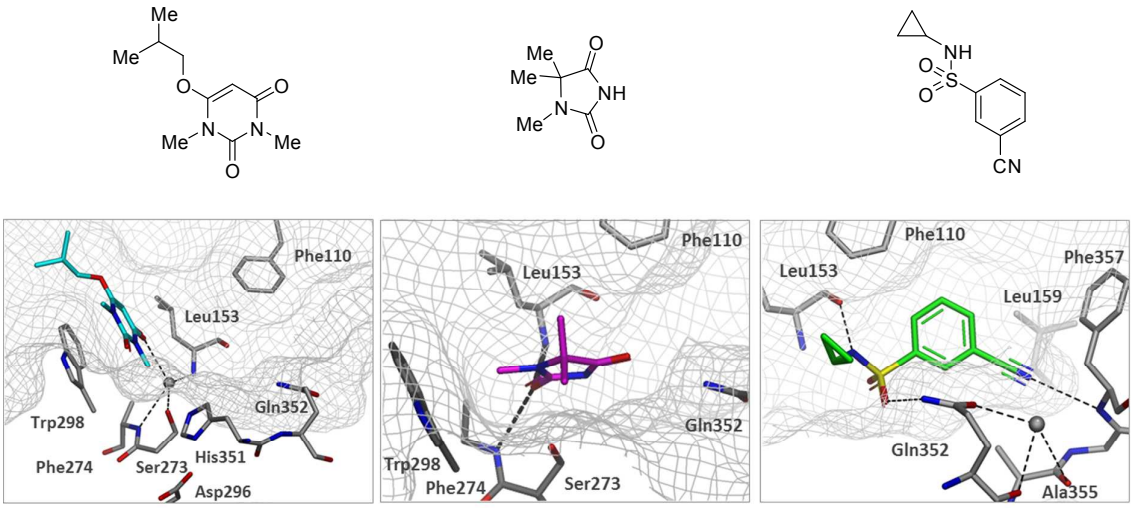

Figure 2. X-ray crystal structures of compounds **2**–**4** bound to Lp-PLA$_2$; uracil **2** (cyan) is a fragment hit that binds adjacent to the catalytic residues Ser273, His351, and Asp296; hydantoin **3** (magenta) is a fragment hit that is bound in the oxyanion hole; and sulfonamide **4** (green) is derived from a fragment hit.[16a] The Connolly surface of the protein is shown as a gray mesh. Selected residues are shown for clarity. The hydrogen bond interactions are shown as dotted lines and water is shown as gray spheres.

PLA2-VIIB is a closely related intracellular phospholipase.[1a, 15] The catalytic sites of Lp-PLA_2 and PLA2-VIIB are highly conserved but in the adjoining groove there are a number of differences including Phe110 (Lp-PLA_2)/Tyr65 (PLA2-VIIB), Gln352 (Lp-PLA_2)/Arg315 (PLA2-VIIB) and Ala355 (Lp-PLA_2)/Thr318 (PLA2-VIIB). Darapladib (**1**) possesses a 1200-fold selectivity for Lp-PLA_2 over PLA2-VIIB, and makes van der Waals contacts with the sidechains of these residues.[16]

One of the goals for this project was to identify novel chemotypes that had comparable activity in plasma assay to darapladib. We reasoned that if we were able to achieve a significant decrease in the drop off between the Lp-PLA_2 biochemical and plasma assays, the lead compound does not need to be picomolar in the biochemical assay. Therefore, the lead compound could have lower molecular weight (MW) and more reasonable lipophilicity than darapladib (MW = 667, clogP[18] = 8.3). Literature has shown that aspiring to keep the physicochemical properties within guidelines is desirable (i.e. MW <500 and clogP <5) through association with increased success in the clinic.[19] However, optimisation against the plasma potency should not be performed without a parallel consideration of *in vivo* parameters and we therefore looked to achieve good pharmacokinetic properties.[20] Additionally, we wished to retain greater than 100-fold selectivity against PLA2-VIIB. We chose to use fragment based technology to meet these goals, as this approach can facilitate tighter control of physicochemical properties.

Our fragment screen methodology and output have been reported previously.[16a] Crystal structures for 50 fragment hits were obtained, and were observed to bind throughout the entire length of the canyon-like groove of Lp-PLA_2 occupying a total length of ~24 Å.

The X-ray crystal structures of three compounds (**2**–**4**) bound to Lp-PLA_2 are superimposed in Figure 1b (and shown separately in Figure 2). These compounds occupy different regions of the binding site and recapitulate many of the key binding interactions of darapladib.[16a] Hydantoin **3** (IC_{50} >1 mM)[21] was perceived to be an attractive starting point. It is a small fragment (heavy atom count = 10), that is synthetically accessible with excellent vectors for exploring the binding pocket. Uracil **2** (IC_{50} ~1 mM)[21] and sulfonamide **4** (IC_{50} ~1 mM)[21] showed potential areas to gain binding affinity, for example hydrogen bonds to Gln352 (sidechain), Leu153 (backbone carbonyl), Leu369 (backbone carbonyl), Phe357 (backbone NH), and lipophilic/π-stacking interactions with the indolyl of Trp298. This letter will disclose how we evolved hydantoin **3**, using insights from uracil **2** and sulfonamide **4**, to generate novel low MW inhibitors of Lp-PLA_2 with a promising PK profile.

RESULTS AND DISCUSSION

Hydantoin Optimisation. Hydantoin **3** (clogP = 0.03) did not show any activity in the biochemical assay, and was only discovered through the X-ray crystallographic screen. The crystal structure shows that the fragment occupies the oxyanion hole of Lp-PLA_2 with two hydrogen bonds to the backbone NH of both Leu153 and Phe274 (Figure 2b).

The overall strategy to develop hydantoin **3** into a potent inhibitor is illustrated in Figure 3. It began by overlaying the crystal structures of hydantoin **3** and sulfonamide **4** bound to Lp-PLA_2 (Figure 1b). These two compounds map out the very bottom of the pocket and a narrow channel is present between the NH of hydantoin **3** and phenyl ring of sulfonamide **4**. Merging these motifs with a suitable linker should simultaneously increase potency and lipophilicity of the hydantoin template. The predicted clash between the sulfonamide oxygen and hydantoin

carbonyl precluded directly linking the two fragments. We employed a virtual screening (VS) strategy to investigate a variety of linkers to grow from hydantoin **3** to areas of known potency (such as regions occupied by uracil **2**, sulfonamide **4** and darapladib).

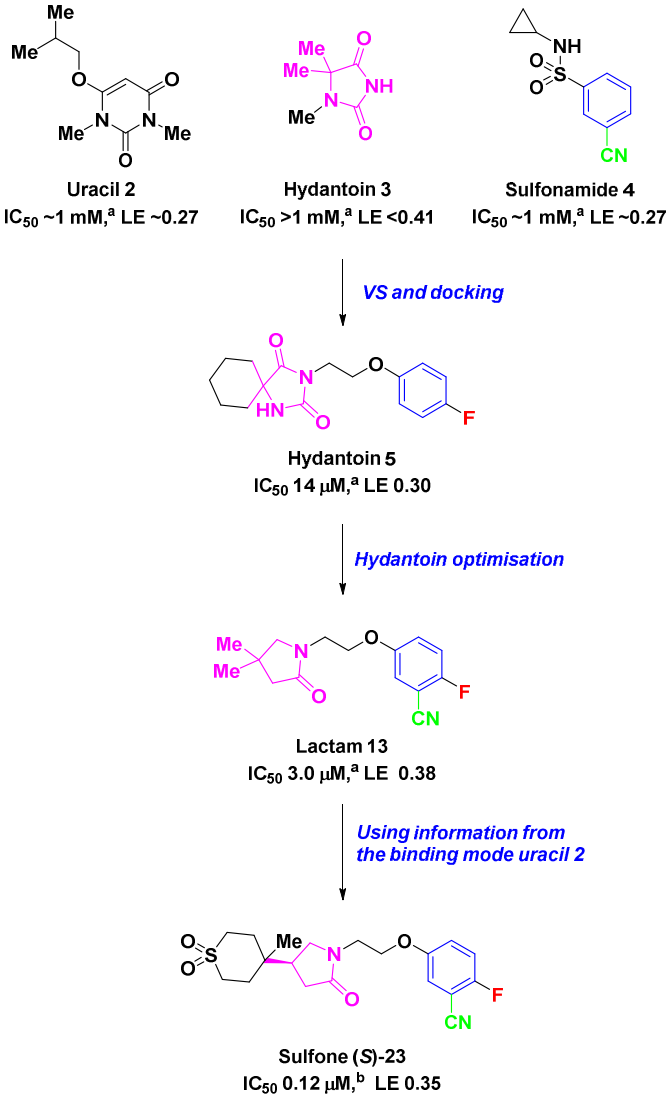

Figure 3. Schematic design process. Moieties within the compounds are coloured according to the original compound they are derived from. [a]rhLp-PLA$_2$ PED6 assay. [b]rhLp-PLA$_2$ Thio-PAF assay.

Substructure screening identified ~16,000 hydantoins from in-house and commercially available compounds. This library was filtered on molecular weight (MW <300), and docking runs were performed against in-house Lp-PLA_2 crystal structures using the Astex proprietary version of Gold software.[22] A total of 33 hits were subsequently screened using X-ray crystallography and biochemical assays. This method quickly identified hydantoin **5** with an IC_{50} = 14 μM[21]. The crystal structure of hydantoin **5** bound in Lp-PLA_2 is shown in Figure 4. The hydantoin forms the expected two H-bonds in the oxyanion hole and the ethoxy linker places the phenyl ring into a deep pocket terminated by residue Phe357. The cyclohexyl ring sits in a predominantly lipophilic groove surrounded by the sidechains of Leu153, Trp298 and Phe322.

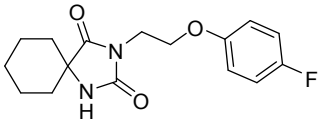

5

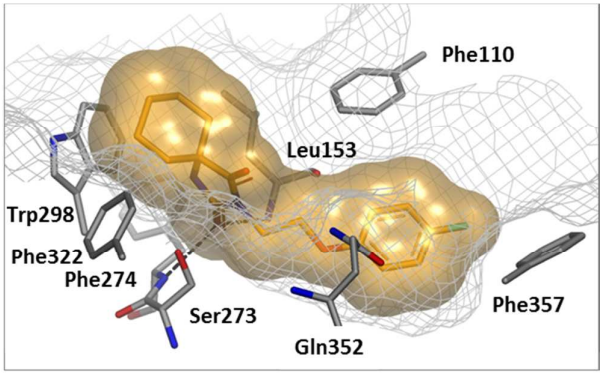

Figure 4. X-ray crystal structure of hydantoin **5** bound in Lp-PLA_2. The Connolly surface of the ligand is shown in solid orange and the protein as a gray mesh. Selected residues are shown for clarity. The hydrogen bond interactions are shown as dotted lines.

Although hydantoin **5** was a reasonably ligand efficient lead with LE = 0.30,[23] we decided to strip back the cyclohexyl ring and optimize the hydantoin motif (Table 1). Hydantoin **6** was designed to retain the *N*-methyl (from hydantoin **3**) and the ethoxy linker (from hydantoin **5**), and was only weakly active at IC_{50} ~1 mM[21]. Addition of the gem-dimethyl in hydantoin **7** gave a ~50-fold increase in potency to IC_{50} = 20 μM[21] (LE = 0.34) and demonstrated that the branched nature of the gem-dimethyl was important. Incorporation of the 4-fluoro in hydantoin **8** gave a modest 2-fold increase in affinity and retained the LE at 0.34. Systematic exploration of the hydantoin ring by removing the *N*-methyl (**9**), and then replacing the amide carbonyl with methylene (**10**), did not yield an improvement in LE over hydantoin **8**. However, replacing the NH by methylene to give γ-lactam **11**, resulted in a more ligand efficient template (LE = 0.38). Ring expansion was also tolerated and yielded δ-lactam **12** with similar potency (IC_{50} = 10 μM[21], LE = 0.36).

Table 1. Structure-Based Optimization of Hydantoin 5

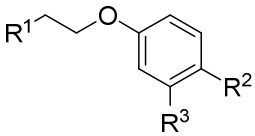

Cpd	R^1	R^2	R^3	MW/clogP	rhLp-PLA_2 PED6 IC_{50} (μM)[a] / LE	rhLp-PLA_2 Thio-Paf IC_{50} (μM)[b] / LE	rhPLA2-VIIB IC_{50} (μM)[c]
5	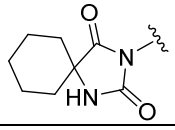	-F	-H	306 / 3.3	14 / 0.30	-	-
6	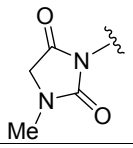	-H	-H	234 / 1.3	~1000 / ~0.24	-	-

Cpd	R^1	R^2	R^3	MW/clogP	rhLp-PLA$_2$ PED6 IC$_{50}$ (μM)[a] / LE	rhLp-PLA$_2$ Thio-Paf IC$_{50}$ (μM)[b] / LE	rhPLA2-VIIB IC$_{50}$ (μM)[c]
7	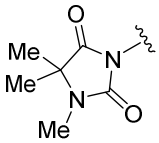	-H	-H	262 / 2.3	20 / 0.34	-	-
8	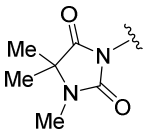	-F	-H	280 / 2.6	10 / 0.34	-	-
9	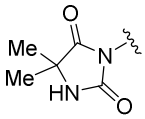	-F	-H	266 / 2.3	44 / 0.31	-	>100
10	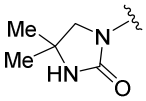	-F	-H	252 / 2.6	39 / 0.33	-	>100
11	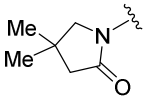	-F	-H	251 / 2.8	11 / 0.38	-	>100
12	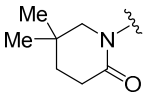	-F	-H	265 / 3.4	10 / 0.36	-	-
13	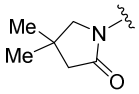	-F	-CN	276 / 2.5	3.0 / 0.38	15 / 0.33	>100

All assay details are described in Supporting Information. [a]Recombinant human Lp-PLA$_2$ PED6 assay. The main Lp-PLA$_2$ bioassay used a Thio-Paf substrate but the assay format was unsuitable for weakly binding compounds (~50 μM or weaker). A PED6 fluorogenic substrate was employed for the weaker inhibitors. These two primary bioassays correlated well across many compounds (data not shown). [b]Recombinant human Lp-PLA$_2$ Thio-PAF assay. [c]Recombinant human PLA2-VIIB Thio-PAF assay.

The crystal structure of sulfonamide **4** bound in Lp-PLA_2 indicates that the cyano fills a small pocket formed by Phe357, Ala355, the sidechain of Leu159 and a water molecule (Figure 2c). The cyano also forms a long H-bond to the backbone NH of Phe357. When the X-ray crystal structures of sulfonamide **4** or hydantoin **5** bound to Lp-PLA_2 are overlaid, both the phenyl rings reside in the same position. We therefore substituted a cyano in the equivalent position on the lactam series leading to the design of lactam **13**, which had an IC_{50} = 3.0 μM[21] and an ITC K_d = 2.0 μM. This compound was potent enough to be characterized in the main Thio-Paf biochemical assay and had an IC_{50} = 15 μM[11] (see Table 1, footnote a).

The crystal structure of lactam **13** in complex with Lp-PLA_2 (Figure 5) gave the expected binding mode and the cyano fills the small sub pocket. The gem-dimethyl motif in lactam **13** provides excellent complementarity to the pocket and completely fills the groove between the sidechains of Leu153, Trp298 and Phe322. The ether oxygen in **13** is important to orientate the phenyl ring into the pocket lined with Phe110, Ala355 and Phe357, and also forms a close contact with the sidechain of Gln352. The residues Phe110, Gln352 and Ala355 are significant because they are replaced in PLA2-VIIB by Tyr, Arg and Thr, respectively. Lactam **13** shows good selectivity over PLA2-VIIB and this template became our lead for further optimisation.

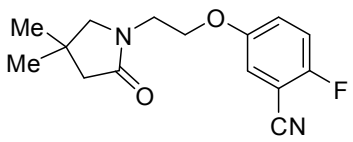

13

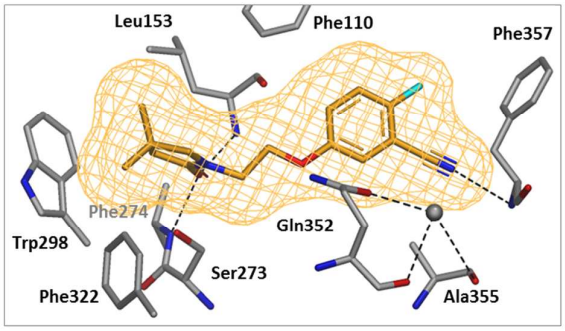

Figure 5. X-ray crystal structure of lactam **13** in complex with Lp-PLA$_2$. The Connolly surface of the ligand is shown as an orange mesh. Selected residues are shown for clarity. The hydrogen bond interactions are shown as dotted lines and a water molecule is shown as a gray sphere.

Growth of lactam 13. The gem-dimethyl in lactam **13** makes contact with the indolyl of Trp298 and fills a lipophilic space between the sidechains of Leu153 and Phe322. Uracil **2** occupies a similar region and stacks on the indolyl of Trp298. We therefore designed lactam **(±)-14** to mimic this interaction by substituting a phenyl ring from the C-4 position on the lactam (Table 2), and designed further analogues with an additional methyl (enantiomers **(*S*)-15** and **(*R*)-15**).

Table 2. Structure-Based Optimization of Lactam 13.

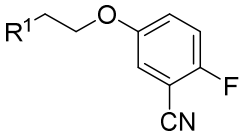

Cpd	R^1	MW/clogP	rhLp-PLA_2 Thio-Paf IC_{50} (μM)[a] / LE	rhPLA2-VIIB IC_{50} (μM)[b]
13	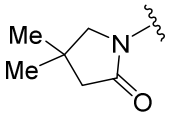	276 / 2.5	15 / 0.33	>100
(±)-14	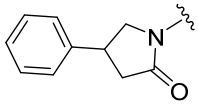	324 / 3.3	0.86 / 0.34	>100
(*S*)-15[c]	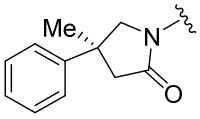	338 / 3.5	1.6 / 0.32	>100
(*R*)-15[c]	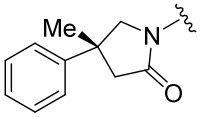	338 / 3.5	1.0 / 0.33	>100

All assay details are described in Supporting Information. [a]Recombinant human Lp-PLA_2 Thio-PAF assay. [b]Recombinant human PLA2-VIIB Thio-PAF assay. [c]Chirality of the stereocentre has been confirmed from the X-ray crystal structure of the ligand bound to Lp-PLA_2.

Lactams **(±)-14**, **(*S*)-15** and **(*R*)-15** all successfully gave an increase in potency of ~15-fold and retained LE. Interestingly, the three analogues were approximately equipotent, and in agreement with available ITC measurements (lactam **(*S*)-15**: K_d = 0.45 μM and lactam ***(R)*-15**: K_d = 0.53 μM). Figure 6 shows the superimposed binding modes of **(*S*)-15** and **(*R*)-15** in complex with Lp-PLA_2. The unsubstituted phenyl rings both form edge-to-face stacking

interactions with the indolyl of Trp298, and the multiple equipotent orientations of the phenyl rings are possible because the groove above Trp298 is wide and lipophilic. Addition of substituents to the phenyl ring or replacement by heterocycles (such as pyridine), did not significantly increase the potency (data not shown) and we sought a better solution to gain potency in this region.

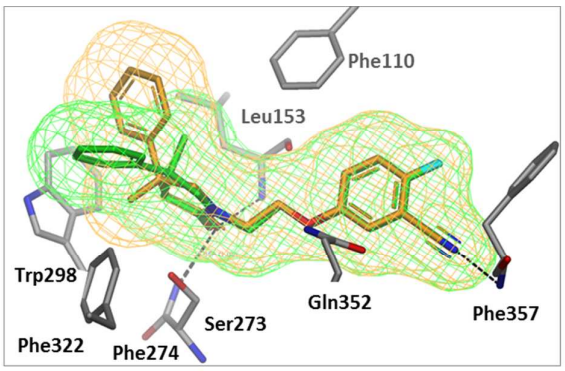

Figure 6. Superposition of the X-ray crystal structures of lactams **(*S*)-15** (green) and **(*R*)-15** (orange), each in complex with Lp-PLA$_2$. The Connolly surfaces of the ligands are shown as a mesh. Selected residues are shown for clarity. The hydrogen bond interactions are shown as dotted lines.

Alongside aromatic substitutions (lactams **(±)-14**, **(*S*)-15** and **(*R*)-15**), we also tried to grow from the template using alkyl groups. A series of compounds were synthesized where we introduced methyl groups to the gem-dimethyl moiety in lactam **13** in order to explore the groove above Trp298 (Table 3). Lactam **(±)-16** gave an 8-fold increase in potency to an IC_{50} = 2.0 μM. Separation of the enantiomers gave lactams **(*S*)-16** and **(*R*)-16**. These enantiomers had a low eudysmic ratio (ratio of these potencies) of 2, and again showed the pocket could accommodate both isomers. Removing the lactam C-4 methyl to generate the *i*-propyl in **(±)-17** gave an equipotent analogue and slightly increased the LE. This LE was maintained by further substitution of the *i*-propyl to give the *t*-butyl **(±)-18** (IC_{50} = 0.98 μM, LE = 0.37). The crystal structure of **(±)-18** in Lp-PLA_2 showed the binding mode was consistent with previous analogues and the *t*-butyl sits in the Leu153, Trp298 and Phe322 groove (Figure 7).

Table 3. Structure-Based Optimization of Lactam 13

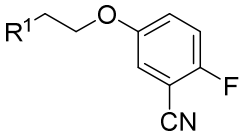

Cpd	R^1	MW / clogP	A: rhLp-PLA$_2$ Thio-Paf IC$_{50}$ (µM)[a] / LE	B: Plasma IC$_{50}$ (µM)[b] / LE	B / A	rhPLA2-VIIB IC$_{50}$ (µM)[c]
13	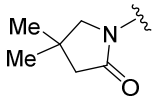	276 / 2.5	15 / 0.33	-	-	>100
(±)-16	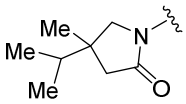	304 / 3.4	2.0 / 0.35	-	-	>100
(*S*)-16[d]	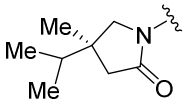	304 / 3.4	2.3 / 0.35	6.2 / 0.32	2.7	>100
(*R*)-16[d]	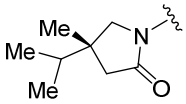	304 / 3.4	5.4 / 0.33	13 / 0.30	2.4	>100
(±)-17	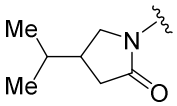	290 / 2.9	1.9 / 0.37	-	-	>100
(±)-18	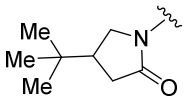	304 / 3.3	0.98 / 0.37	5.1 / 0.33	5.2	>100
(±)-19[e]	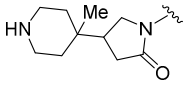	345 / 2.1	0.62 / 0.34	0.87 / 0.33	1.4	>100

All assay details are described in Supporting Information. [a]Recombinant human Lp-PLA$_2$ Thio-PAF assay. [b]Lp-PLA$_2$ in whole human plasma Thio-PAF assay. [c]Recombinant human PLA2-VIIB Thio-PAF assay. [d]Chirality of the stereocentre has been confirmed from the X-ray crystal structure of the ligand bound to Lp-PLA$_2$. [e]Formate salt.

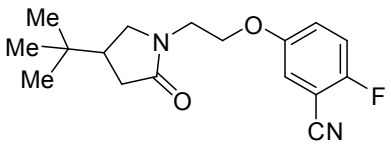

(±)-18

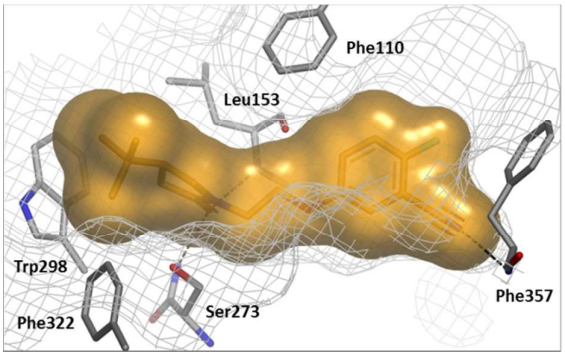

Figure 7. X-ray crystal structure of Lp-PLA$_2$ in complex with the (*S*)-enantiomer of **(±)-18**. The Connolly surface of the ligand is shown in solid orange and the protein as a gray mesh. Selected residues are shown for clarity. The hydrogen bond interactions are shown as dotted lines.

We felt the interactions between the *t*-butyl in **(±)-18** with the sidechains of Trp298, Leu153 and Phe322 might be improved by cyclising into a ring. We initially chose a piperidine ring where the NH group would point towards solvent and allow modulation of physicochemical properties of the molecule. The basic moiety in lactam **(±)-19** was tolerated and had an IC$_{50}$ = 0.62 μM.

Lactams **13–19** were selective over PLA2-VIIB (Table 3) and all had IC$_{50}$ >100 μM. These compounds also showed good activity in the plasma assay, and the drop off between the Lp-PLA$_2$ assay and the plasma assay remained extremely low (≤5-fold). This represented a

significant improvement over darapladib (710-fold ratio, Table 4). We attributed this result to the relatively low lipophilicity of this series (clogP ≤3.4), and the chromLogD$_{7.4}$ of lactam **(±)-19** was measured to be 1.5. Lactam **(±)-19** became our lead template for further exploration and assessment of the PK profile of the series.

Optimisation of (±)-19. The secondary amine **(±)-19** had a potency of IC_{50} = 0.62 μM and comparable activity in the plasma assay. The amino group of the piperidine is too far away from the indolyl face of Trp298 to from a productive cation-π interaction and so we explored alternatives. Exchanging the amine for an ether gave lactam **(±)-20**, which is an uncharged analogue at physiological pH, and showed a 4-fold increase in potency in the Lp-PLA_2 bioassay. Acylation of the amine **(±)-19** to give amide **(±)-21** did not yield further potency, but interestingly, methylation to the tertiary amine **(±)-22** improved the potency by 8-fold to IC_{50} = 0.075 μM. The enantiomers where chirally separated to give **(*S*)-22** and **(*R*)-22**, which had IC_{50} of 0.072 μM and 2.7 μM respectively. The eudysmic ratio is now 38, and this is significantly higher than the ratio of ~2 for the previous pairs (i.e. **(*S*)-15**/**(*R*)-15**, and **(*S*)-16**/**(*R*)-16**). The (*R*)-enantiomer of **22** is the distomer (the less active isomer), and although the compound is accommodated in the pocket, the interactions with the protein are inferior with respect to the (*S*)-enantiomer of **22**.

Table 4. Structure-Based Optimization of Lactam (±)-19

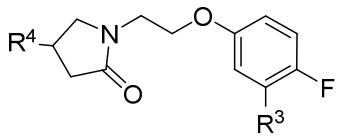

Cpd	R^4	R^3	MW / clogP / Chrom $LogD_{7.4}$	A: rhLp-PLA_2 Thio-Paf IC_{50} (μM)[a] / LE	B: Plasma IC_{50} (μM)[b] / LE	B / A	rhPLA2-VIIB IC_{50} (μM)[c]
(±)-19[d]	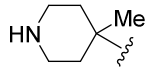	-CN	345 / 2.1 / 1.5	0.62 / 0.34	0.87 / 0.33	1.4	>100
(±)-20	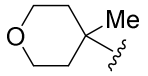	-CN	346 / 2.1 / 3.7	0.16 / 0.37	0.26 / 0.36	1.6	>100
(±)-21	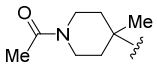	-CN	387 / 1.2 / 2.9	0.25 / 0.32	0.66 / 0.30	2.6	>100
(±)-22	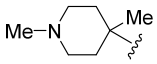	-CN	359 / 2.6 / -	0.075 / 0.37	0.27 / 0.34	3.6	>10
(*S*)-22[e]	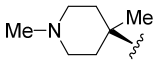	-CN	359 / 2.6 / -	0.072 / 0.37	0.20 / 0.35	2.8	8.0
(*R*)-22[e]	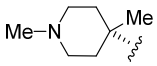	-CN	359 / 2.6 / 1.7	2.7 / 0.29	7.9 / 0.27	2.9	>100
(±)-23	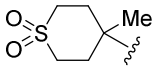	-CN	394 / 0.75 / 2.8	0.18 / 0.34	0.11 / 0.35	0.6	>100
(*S*)-23[f]	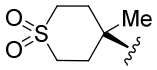	-CN	394 / 0.75 / 3.0	0.12 / 0.35	0.032 / 0.38	0.3	>100
(*R*)-23[f]	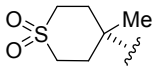	-CN	394 / 0.75 / 2.8	4.3 / 0.27	6.3 / 0.26	1.5	>100

Cpd	R^4	R^3	MW / clogP / Chrom $LogD_{7.4}$	A: rhLp-PLA_2 Thio-Paf IC_{50} (µM)[a] / LE	B: Plasma IC_{50} (µM)[b] / LE	B / A	rhPLA2-VIIB IC_{50} (µM)[c]
(±)-24	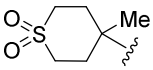	-F	387 / 1.2 / 3.4	0.16 / 0.36	0.29 / 0.34	1.8	>100
(*S*)-24[f]	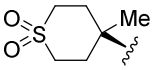	-F	387 / 1.2 / 3.4	0.086 / 0.37	0.10 / 0.37	1.2	>100
(±)-25	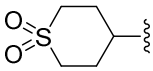	-CN	380 / 0.49 / -	3.9 / 0.28	7.9 / 0.27	2.0	>100
(±)-26	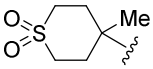	-H	369 / 1.1 / 3.1	0.76 / 0.33	1.5 / 0.32	2.0	>100
1	Darapladib		667 / 8.3 / 6.3	0.000049 / 0.30	0.035 / 0.22	710	0.063

All assay details are described in Supporting Information. [a]Recombinant human Lp-PLA_2 Thio-PAF assay. [b]Lp-PLA_2 in whole human plasma Thio-PAF assay. [c]Recombinant human PLA2-VIIB Thio-PAF assay. [d]Formate salt. [e]Chirality of the stereocentre is inferred from the X-ray crystal structure of the eutomer from the racemic mixture bound to Lp-PLA_2. [f]Chirality of the stereocentre has been confirmed from the X-ray crystal structure of the ligand bound to Lp-PLA_2, and agrees with the crystal structure of the eutomer from the racemic mixture bound to Lp-PLA_2.

Next, we chose to exchange the secondary amine in **(±)-19** for a sulfone (**(±)-23**). We rationalized that the electron withdrawing capability of the sulfone may polarize the adjacent CH's which are in contact with the electron rich indolyl of Trp298 and improve the interaction. Sulfone **(±)-23** showed a small increase in potency (3-fold) in the Lp-PLA_2 assay, but a larger increase in potency in the plasma assay to IC_{50} = 110 nM (8-fold). The enantiomers **(*S*)-23** and **(*R*)-23** also showed a separation in potency in the Lp-PLA_2 assay (eudysmic ratio of 36) and the eutomer (more active isomer) **(*S*)-23** had an IC_{50} = 120 nM. Lactam **(*S*)-23** is equipotent to darapladib in the plasma assay but with a vastly improved LE (LE = 0.38 for **(*S*)-23**, and LE = 0.22 for darapladib). Turning our attention back to the phenyl ring we found that the cyano could be replaced by an equipotent fluorine (**(±)-24** and **(*S*)-24**).

Throughout the optimisation, selectivity over PLA2-VIIB was retained (Table 4) and the ratio between plasma assay and the Lp-PLA_2 Thio-Paf assay remained low (<4). Overall, the LE was maintained at 0.35–0.37 for this set of compounds (in the Lp-PLA_2 Thio-Paf assay).

An important feature of the compounds in Table 4 is the quaternary methyl group on the six-membered aliphatic ring. Comparison of **(±)-23** with the des-methyl sulfone **(±)-25** shows the methyl group engenders a 22-fold increase in potency. QM calculations exploring the torsional landscape around the bond joining the two saturated rings in **(±)-23** and **(±)-25** were performed, and showed both molecules possessed the same lowest energy conformation that is also observed in the bioactive conformation. Thus, the potency gain is presumably through significantly improved ligand-protein complimentary in the Leu153, Trp298 and Phe322 groove. This methyl was only discovered by moving away from aromaticity and careful stepwise optimisation of the gem-dimethyl moiety (**13**) into the *t*-butyl (**(±)-18**). By way of

comparison, the cyano contributes a useful but less spectacular 4-fold increase in potency (comparing **(±)-23** and **(±)-26**). Contributions of different parts of sulfone **(±)-23** to potency are shown in Figure 8 together with their group efficiency (GE).[24] Each moiety analysed has a good contribution to the potency, with the least group efficient moiety being the sulfone which occupies a region that is more solvent exposed.

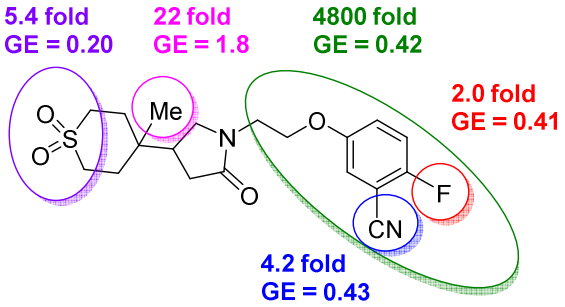

Figure 8. Group efficiency (GE = kcal mol^{-1} per non-hydrogen atom) schematic for compound **(±)-23** based on pairwise comparisons (see Supporting Information). GE ≥0.3 is considered desirable.[24]

Figure 9 shows the crystal structure of **(*S*)-23** bound in Lp-PLA$_2$ with the expected binding mode. Figure 10a superimposes the X-ray crystal structures of **(*S*)-23** in complex Lp-PLA$_2$ with compounds **2**–**4**, and Figure 10b superimposes the X-ray crystal structures of **(*S*)-23** and darapladib. Together these figures show that compounds **2**–**4**, **(*S*)-23** and darapladib (**1**) have common pharmacophore elements, such as the carbonyl that occupies the oxyanion hole and a phenyl ring that resides in the deep lipophilic pocket beside Phe357. Additionally, sulfone **(*S*)-23** has efficiently utilized the space along the bottom of the pocket between Trp298 and Phe357 that was contacted by compounds **2**–**4**; in particular, we exploited the groove above Trp298 (which was not utilized by darapladib) to improve potency and simultaneously

modulate the physicochemical properties of the ligand. Finally, we avoided using areas that were less likely to yield potency such as the region occupied by the (2-aminoethyl)diethylamine moiety in darapladib.

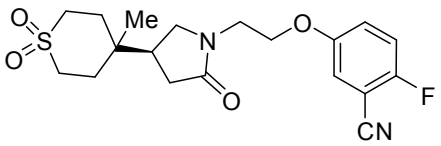

(*S*)-23

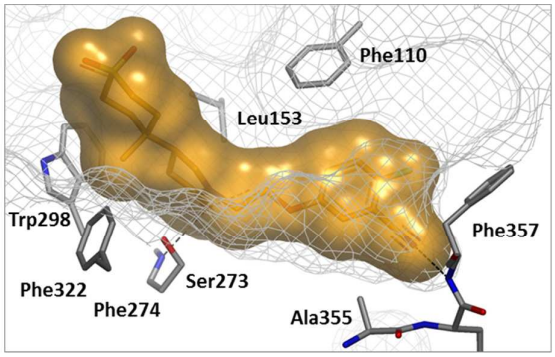

Figure 9. X-ray crystal structure of Lp-PLA$_2$ in complex with lactam **(*S*)-23**. The Connolly surface of the ligand is shown in solid orange and the protein as a gray mesh. Selected residues are shown for clarity. Hydrogen bond interactions are represented as dotted lines.

(a) **(b)**

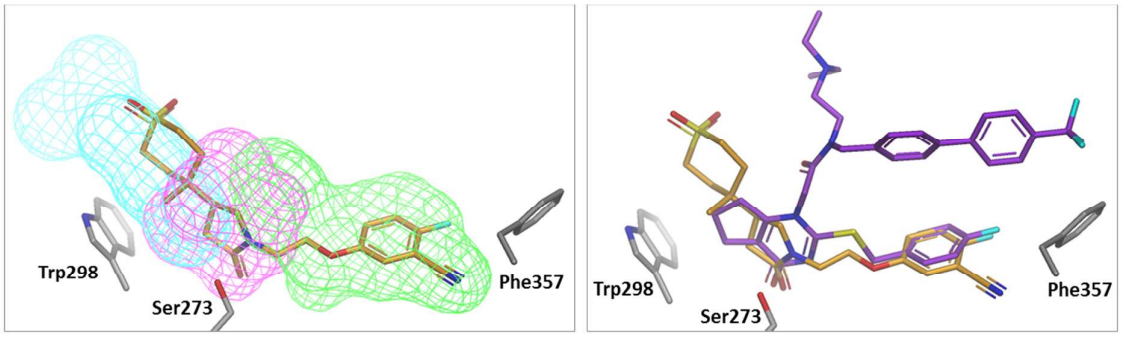

Figure 10. (**a**) Superposition of the X-ray crystal structures of uracil **2** (cyan), hydantoin **3** (magenta) and sulfonamide **4** (green) (only showing the Connolly surface as a mesh), and

(*S*)-23 (orange), bound in Lp-PLA_2. (**b**) Superposition of the crystal structures of **(*S*)-23** (orange) and darapladib (purple) bound in Lp-PLA_2. Only selected residues are shown for clarity.

PK Discussion. Lactams **(±)-19**, **(±)-22**, **(*S*)-23** and **(*S*)-24** are all low MW (<400 MW) compounds, with solubilities >240 μM in the CLND assay (Table 5); in particular **(*S*)-23** was measured by quantitative NMR to be fully soluble at 3.5 mM. The plasma protein binding (PPB) in both rat and dog are extremely low for these compounds, and helps to explain why the drop off between the Lp-PLA_2 assay and the plasma assay is so small (Table 4). The series does not show significant inhibition of the CYP450's 1A2, 3A4, 2C9, 2C19 and 2D6, as exemplified by CYP450 3A4 data in Table 5, where the compounds have an IC_{50} >50 μM. However, there is a difference between the compounds in the permeability assay where the secondary amine **(±)-19** is poor, but the tertiary amine **(±)-22** and sulfones **(*S*)-23 and (*S*)-24** perform better. Assessment of the stability of **(±)-23** in rat blood showed the compound was 100% stable.

Table 5: In Vitro Profile for Key Compounds

Cpd	Structure	MW / clogP / ChromLogD$_{7.4}$	CLND Solubility (µM)	Rat PPB (%)[a]	Dog PPB (%)[a]	CYP450 3A4 IC_{50} (µM)[b]	Pampa Permeability (nm/s)
(±)-19[c]	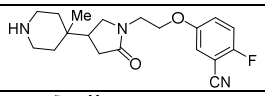	345 / 2.1 / 1.5	242	19	-	> 50	< 3[e]
(±)-22	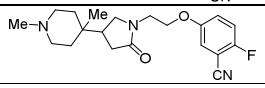	359 / 2.6 / 1.7[d]	> 396	29[c]	44	> 50	210[e]
(*S*)-23	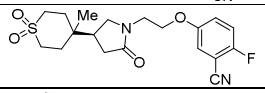	394 / 0.75 / 3.0	> 509	20	25	>50	36[e]
(*S*)-24	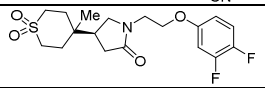	387 / 1.2 / 3.4	> 450	30	-	>50	170[e]
1	Darapladib	667 / 8.3 / 6.3	8	-	-	-	230[f]

[a]3–6 replicates tested at 10 µM. [b]Inhibition of CYP3A4, ≥2 replicates. [c]HCl salt. [d](*R*)-enantiomer tested. [e]Measured at pH = 7.4. [f]Measured at pH = 7.05.

The secondary amine **(±)-19** is a low *in vivo* clearance compound in rat (Table 6) with a reasonable volume of distribution (Vss) and half-life ($T_{1/2}$); this is in part attributed to the basic centre in the molecule. However, amine **(±)-19** has poor permeability in the PAMPA assay which translates into an extremely low bioavailability. In contrast, the tertiary amine **(±)-22** is a moderate clearance compound (Cl = 24 mL/min/kg), and its superior permeability leads to good oral bioavailability (%F = 52%).

Sulfone **(*S*)-23** has a low intrinsic clearance of 1.1 mL/min/g in rat liver microsomes. Unfortunately, this does not translate *in vivo* where it shows a much higher clearance of 67 mL/min/kg (Table 6). However, modulation of the rat clearance is possible as demonstrated by sulfone **(±)-24**.

When assessed in dog, the PK profile of **(±)-22** and **(*S*)-23** look similar, and are both low clearance compounds (8.6 and 11 mL/min/kg, respectively). **(±)-22** shows good oral bioavailability (%F = 76%), although has a shorter half-life than desired. Overall, the series shows a promising profile and provides a suitable starting point for further lead optimization.

Table 6: *In Vivo* Profile of Key Compounds in Rat and Dog

Cpd	Structure	Rat				Dog			
		Cl (mL/min /kg)	$T_{1/2}$ (hr)	Vss (L/kg)	%F oral (%)	Cl (mL/min /kg)	$T_{1/2}$ (hr)	Vss (L/kg)	%F oral (%)
(±)-19[a]	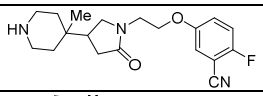	15	2.4	2.0	< 5	-	-	-	-
(±)-22[a]	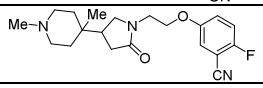	24	1.8	3.2	52	8.6	3.2	2.5	76
(*S*)-23	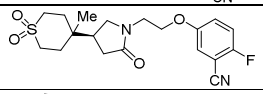	67	0.34	1.2	-	11	1.3	1.3	-
(±)-24	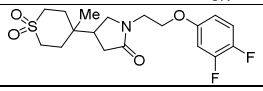	22	0.35	0.63	47	-	-	-	-

[a]In rat, HCl salt.

Synthesis. Synthesis of sulfone **(±)-23** is laid out in Schemes 1 and 2, and followed the convergent strategy which involved a late stage alkylation of 2-pyrroldinone **(±)-30** with methanesulfonate **32**.

Construction of 2-pyrroldinone **(±)-30** was central to this synthesis, and was generated in four steps from commercially available thiane-4-carbaldehyde (Scheme 1). Thiane-4-carbaldehyde was methylated with MeI and NaH to generate the quaternary carbon center in **27**. This was followed by a Horner−Wadsworth−Emmons reaction with triethyl phosphonoacetate and *t*-BuOK to give (*E*)-unsaturated ester **28**. Nitromethane was reacted with the conjugated ester through a Michael addition to generate γ-nitro ester **(±)-29**. The nitro group was then selectively reduced with $NiCl_2$ and $NaBH_4$, and *in situ* cyclisation of the resulting γ-amino ester directly afforded 2-pyrrolidone **(±)-30**.

Scheme 1. Synthesis of lactam Intermediate (±)-31[a]

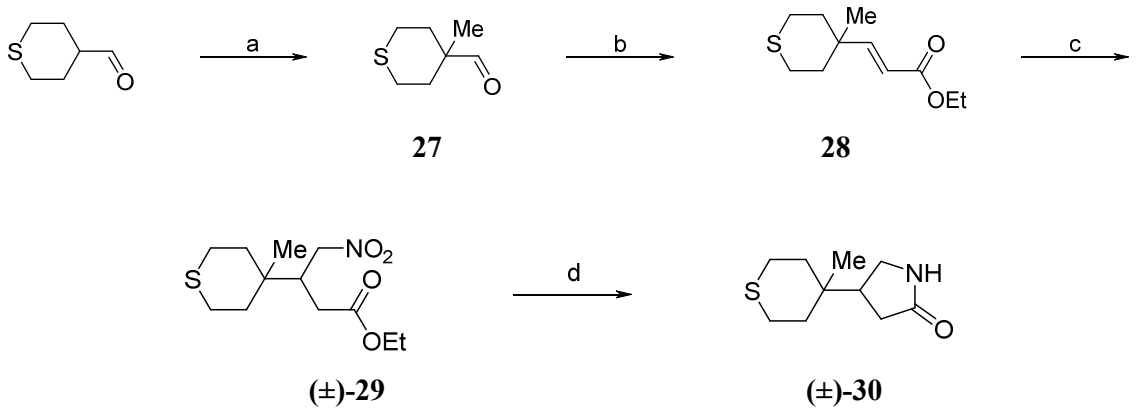

[a]Reagents and conditions: (a) MeI, *t*-BuOK, THF, 0 °C, 2 h, 94%; (b) Triethyl phosphonoacetate, *t*-BuOK, THF, 0 °C, 3 h, 96%; (c) Nitromethane, 1,1,3,3-tetramethylguanidine, 100 °C (microwave), 4 h, 43%; (d) $NiCl_2 \cdot 6H_2O$, $NaBH_4$, MeOH, 0 °C, 1.5 h, 65%.

Methanesulfonate **32** was prepared in two steps from the commercially available 2-fluoro-5-hydroxybenzonitrile (Scheme 2). 2-Fluoro-5-hydroxybenzonitrile was coupled with ethylene carbonate in the presence of K_2CO_3 to give alcohol **31** in a high yield. This was treated with methanesulfonyl chloride and triethylamine to give methanesulfonate **32**. Alkylation of 2-pyrrolidine **(±)-30** with **32** proceeded smoothly at elevated temperatures to afford sulfide **(±)-33** in 44% yield. Finally, oxidation of **(±)-33** with mCPBA gave sulfone **(±)-23**.

Scheme 2. Synthesis of Sulfone (±)-23[a]

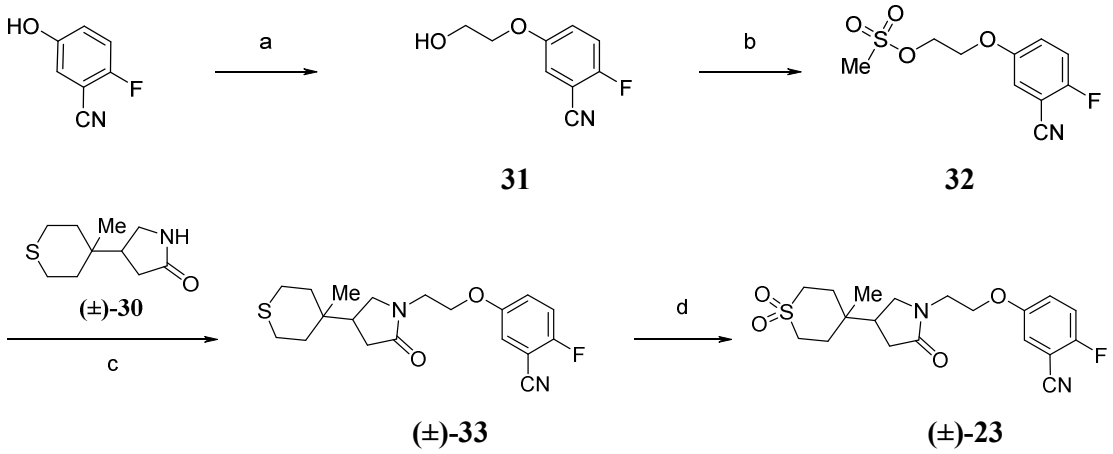

[a]Reagents and conditions: (a) Ethylene carbonate, K_2CO_3, DMF, 110 °C, 18 h, 92%; (b) Ms-Cl, Et_3N, THF, 0 °C, 0.5 h, 88%; (c) NaH, DMF, 40 °C, 18 h, 44%; (d) mCPBA, DCM, 25 °C, 4 h, 66%.

CONCLUSION

In summary, we have discovered a new γ-lactam chemotype that binds in the oxyanion hole of Lp-PLA_2, and which is distinct from the known pyrimidinone core. Previous inhibitors[9-10, 14] and analyses of the binding site[16] have suggested that obtaining potent, low lipophicity inhibitors could represent a significant challenge. Using a fragment-based approach we have identified sulfone **(*S*)-23**, which shows a similar potency in plasma to darapladib but has significantly lower MW and is less lipophilic.

The design began with a hydantoin fragment that represented a novel chemotype for interacting with the oxyanion hole. Analysis of other diverse fragments that bound near the oxyanion hole was used to guide a virtual screening approach. This identified hydantion **5** which contained two pharmacophore elements (the hydantoin carbonyl and a phenyl ring)

joined by an ethoxy linker. Simplification of compound **5** and further optimisation of the hydantoin motif generated the more ligand efficient γ-lactam **11**. Subsequent stepwise growth of the lactam into the Trp298 groove allowed us to further optimize ligand-protein interactions and discover a key methyl that was essential for potency. The resulting sulfone **(*S*)-23** is an alternative low MW, potent and selective inhibitor for Lp-PLA_2 with attractive PK properties.

EXPERIMENTAL SECTION

Chemistry. Compounds **2**–**5** are commercially available. General directions are described in the Supporting Information. The synthesis and characterisation of sulfones **(±)-23**, **(*S*)-23** and **(*R*)-23** are described below. A full description of the synthetic protocols and chemical characterizations for compounds **2**–**22** and **24**–**26** can be found in the Supporting Information. The purity of each compound was analysed by HPLC−MS (ESI) and is >95%, unless otherwise stated.

Procedures.

Synthesis of 2-fluoro-5-{2-[4-(4-methyl-1,1-dioxo-1λ^6-thian-4-yl)-2-oxopyrrolidin-1-yl]ethoxy}benzonitrile ((±)-23), 2-fluoro-5-{2-[(4*R*)-4-(4-methyl-1,1-dioxo-1λ^6-thian-4-yl)-2-oxopyrrolidin-1-yl]ethoxy}benzonitrile ((*R*)-23) and 2-fluoro-5-{2-[(4*S*)-4-(4-methyl-1,1-dioxo-1λ^6-thian-4-yl)-2-oxopyrrolidin-1-yl]ethoxy}benzonitrile ((*S*)-23).

2-Fluoro-5-{2-[4-(4-methyl-1,1-dioxo-1λ^6-thian-4-yl)-2-oxopyrrolidin-1-yl]ethoxy}benzonitrile ((±)-23). A mixture of 4-(4-methylthian-4-yl)pyrrolidin-2-one (**(±)-30**) (1000 mg, 5.02 mmol) and 2-(3-cyano-4-fluorophenoxy)ethyl methanesulfonate (**32**)

(1951 mg, 7.53 mmol) were stirred in DMF (8 mL). NaH (502 mg, 12.5 mmol, 60% in mineral oil) was slowly added. The reaction was slowly warmed to 40 °C and stirred overnight. The reaction was quenched with water and the product was extracted with EtOAc (x1). The organic layer was separated and then washed with brine and evaporated *in vacuo*. The crude product was purified by preparative TLC (100% EtOAc) to give 2-fluoro-5-{2-[4-(4-methylthian-4-yl)-2-oxopyrrolidin-1-yl]ethoxy}benzonitrile (**(±)-33**) (800 mg, 44%). To 2-fluoro-5-{2-[4-(4-methylthian-4-yl)-2-oxopyrrolidin-1-yl]ethoxy}benzonitrile (**(±)-33**) (250 mg, 0.690 mmol) was added 3-chloroperoxybenzoic acid (476 mg, 2.76 mmol) and DCM (5 mL). The reaction was stirred at 25 °C for 4 hours. The reaction was quenched by addition of sat. aqueous $Na_2S_2O_3$ and the product was extracted with EtOAc (x1). The organic layer was separated and washed with brine and evaporated *in vacuo*. The product was purified by preparative HPLC to yield 2-fluoro-5-{2-[4-(4-methyl-1,1-dioxo-1λ^6-thian-4-yl)-2-oxopyrrolidin-1-yl]ethoxy}benzonitrile (**(±)-23**) as a colourless solid (180 mg, 66%). ^{1}H NMR (CD_3OD): δ 7.36–7.32 (m, 1H), 7.32–7.26 (m, 2H), 4.19 (t, *J* = 5.3 Hz, 2H), 3.73 (dt, *J* = 14.6, 5.2 Hz, 1H), 3.68–3.57 (m, 2H), 3.49 (dd, *J* = 10.2, 7.4 Hz, 1H), 3.20–3.10 (m, 2H), 3.05–2.95 (m, 2H), 2.56 (app quin, *J* = 8.6 Hz, 1H), 2.42 (dd, *J* = 17.0, 9.1 Hz, 1H), 2.35 (dd, *J* = 17.0, 9.1 Hz, 1H), 2.04–1.94 (m, 2H), 1.89–1.80 (m, 2H), 1.04 (s, 3H). ^{13}C NMR (CD_3OD): δ 175.3, 157.8 (d, *J* = 250.1 Hz), 154.9 (d, *J* = 2.2 Hz), 122.1 (d, *J* = 7.3 Hz), 117.7, 117.1 (d, *J* = 21.3 Hz), 113.2, 101.0 (d, *J* = 17.6 Hz), 66.3, 48.8, 46.4, 41.8, 39.7, 32.9, 32.7, 32.2, 31.6, 17.3. LCMS (method 2): *m/z* $[M+H]^+$ 412, RT = 1.25 min. Purity >95%. HRMS (ESI-QTOF): *m/z* $[M+H]^+$ calculated for $C_{19}H_{23}FN_2O_4S$ is 395.1435; Found 395.1438 (Δ = 0.89 ppm).

The product was chirally separated by preparative-SFC to give 2-fluoro-5-{2-[(4*R*)-4-(4-methyl-1,1-dioxo-1λ^6-thian-4-yl)-2-oxopyrrolidin-1-yl]ethoxy}benzonitrile (**(*R*)-23**) as an off

white solid (75 mg, 42% recovery) and 2-fluoro-5-{2-[(4*S*)-4-(4-methyl-1,1-dioxo-1λ^6-thian-4-yl)-2-oxopyrrolidin-1-yl]ethoxy}benzonitrile (**(*S*)-23**) as a colourless solid (78 mg, 43% recovery).

2-Fluoro-5-{2-[(4*S*)-4-(4-methyl-1,1-dioxo-1λ^6-thian-4-yl)-2-oxopyrrolidin-1-yl]ethoxy}benzonitrile ((*S*)-23). ^{1}H NMR (CD_3OD): δ 7.36–7.32 (m, 1H), 7.32–7.26 (m, 2H), 4.19 (t, *J* = 5.3 Hz, 2H), 3.73 (dt, *J* = 14.6, 5.2 Hz, 1H), 3.68–3.57 (m, 2H), 3.48 (dd, *J* = 10.2, 7.5 Hz, 1H), 3.20–3.10 (m, 2H), 3.05–2.95 (m, 2H), 2.56 (app quint, *J* = 8.6 Hz, 1H), 2.42 (dd, *J* = 17.0, 9.1 Hz, 1H), 2.35 (dd, *J* = 17.0, 9.1 Hz, 1H), 2.04–1.94 (m, 2H), 1.89–1.79 (m, 2H), 1.04 (s, 3H). ^{13}C NMR (CD_3OD): δ 175.3, 157.8 (d, *J* = 249.4 Hz), 154.9 (d, *J* = 2.2 Hz), 122.1 (d, *J* = 8.1 Hz), 117.7, 117.1 (d, *J* = 22.0 Hz), 113.2, 100.9 (d, *J* = 16.9 Hz), 66.3, 48.8, 46.4, 41.7, 39.7, 32.9, 32.7, 32.2, 31.6, 17.3. LCMS (method 2): *m/z* $[M+H]^+$ 412, RT = 1.24 min. Purity >95%. HRMS (ESI-QTOF): *m/z* $[M+H]^+$ calculated for $C_{19}H_{23}FN_2O_4S$ is 395.1435; Found 395.1430 (Δ = -1.25 ppm). *ee* >99%. Chirality of the stereocentre has been confirmed from the X-ray crystal structure of the ligand bound to Lp-PLA$_2$.

2-Fluoro-5-{2-[(4*R*)-4-(4-methyl-1,1-dioxo-1λ^6-thian-4-yl)-2-oxopyrrolidin-1-yl]ethoxy}benzonitrile ((*R*)-23). ^{1}H NMR (CD_3OD): δ 7.36–7.32 (m, 1H), 7.32–7.26 (m, 2H), 4.19 (t, *J* = 5.3 Hz, 2H), 3.74 (dt, *J* = 14.6, 5.2 Hz, 1H), 3.68–3.57 (m, 2H), 3.49 (dd, *J* = 10.2, 7.4 Hz, 1H), 3.20–3.10 (m, 2H), 3.05–2.95 (m, 2H), 2.56 (app quin, *J* = 8.6 Hz, 1H), 2.42 (dd, *J* = 17.0, 9.1 Hz, 1H), 2.35 (dd, *J* = 17.0, 9.1 Hz, 1H), 2.04–1.94 (m, 2H), 1.89–1.81 (m, 2H), 1.04 (s, 3H). ^{13}C NMR (CD_3OD): δ 175.3, 157.8 (d, *J* = 250.1 Hz), 154.9 (d, *J* = 2.2 Hz), 122.1 (d, *J* = 8.1 Hz), 117.7, 117.1 (d, *J* = 22.0 Hz), 113.2, 100.9 (d, *J* = 16.9 Hz), 66.2, 48.8, 46.4, 41.8, 39.7, 32.9, 32.7, 32.2, 31.6, 17.3. LCMS (method 2): *m/z* $[M+H]^+$ 412, RT =

1.23 min. Purity >95%. HRMS (ESI-QTOF): *m/z* $[M+H]^+$ calculated for $C_{19}H_{23}FN_2O_4S$ is 395.1435; Found 395.1430 (Δ = -1.09 ppm). *ee* >99%.

4-Methylthiane-4-carbaldehyde (27). A stirred solution of thiane-4-carbaldehyde (0.90 g, 6.91 mmol) in THF (23 mL) was cooled in an ice-water bath and then *t*-BuOK (0.93 g, 8.30 mmol) was added. After 10 minutes, MeI (0.67 mL, 10.8 mmol) was added neat. The mixture was stirred with cooling for 2 hours. The reaction was quenched with sat. aquoeus NH_4Cl and the product was extracted with DCM (x3). The combined organic layers were washed with brine, dried over $MgSO_4$, filtered and evaporated *in vacuo* to yield 4-methylthiane-4-carbaldehyde (**27**) as a colourless oil (0.94 g, 94%). The product was used in the next step without further purification. ^{1}H NMR ($CDCl_3$): δ 9.42 (s, 1H), 2.72–2.53 (m, 4H), 2.25–2.15 (m, 2H), 1.72–1.62 (m, 2H), 1.07 (s, 3H). ^{13}C NMR ($CDCl_3$): δ 205.2, 45.5, 33.5, 24.6, 22.2. Purity 90%. HRMS (ESI-QTOF): *m/z* $[M+H]^+$ calculated for $C_7H_{12}OS$ is 145.0680; Found 145.0680 (Δ = 0.26 ppm).

Ethyl (2*E*)-3-(4-methylthian-4-yl)prop-2-enoate (28). A stirred solution of *t*-BuOK (1.32 g, 11.7 mmol) in THF (20 mL) was cooled in an ice-water bath, and then triethyl phosphonoacetate (2.03 mL, 12.3 mmol) was added. After 30 minutes, 4-methylthiane-4-carbaldehyde (**27**) (0.94, g, 5.87 mmol, 90% pure) was added in THF (9 mL). The reaction was stirred for 3 hours, and then quenched with sat. aqueous NH_4Cl. After further dilution with water, the product was extracted with DCM (x3). The combined organic layers were washed with water and brine, dried over $MgSO_4$, filtered and evaporated *in vacuo*. The product was purified by flash chromatography (gradient elution with 0–20% EtOAc/petrol) to yield ethyl (2*E*)-3-(4-methylthian-4-yl)prop-2-enoate (**28**) as a colourless oil (1.2 g, 96%). ^{1}H NMR ($CDCl_3$): δ 6.90 (d, *J* = 16.2 Hz, 1H), 5.79 (d, *J* = 16.2 Hz, 1H), 4.22 (q, *J* = 7.1 Hz,

2H), 2.70–2.59 (m, 4H), 1.93 (ddd, *J* = 13.9, 7.1, 3.7 Hz, 2H), 1.74 (ddd, *J* = 13.9, 8.2, 3.9 Hz, 2H), 1.32 (t, *J* = 7.1 Hz, 3H), 1.09 (s, 3H). ^{13}C NMR ($CDCl_3$): δ 166.9, 156.5, 119.2, 60.4, 37.8, 35.9, 26.6, 24.2, 14.3. Purity 90%.

Ethyl 3-(4-methylthian-4-yl)-4-nitrobutanoate ((±)-29). To a mixture of ethyl (2*E*)-3-(4-methylthian-4-yl)prop-2-enoate (**28**) (1.80 g, 8.40 mmol), nitromethane (5.1 g, 84.0 mmol) was added 1,1,3,3-tetramethylguanidine (967 mg, 8.40 mmol). The reaction was heated at 100 °C (microwave) for 4 hours, and then left at ambient temperature overnight. The mixture was diluted with 2M HCl and the product was extracted EtOAc (x1). The organic layer was separated washed with water, dried with brine and evaporated *in vacuo*. The crude product was purified by preparative TLC (10:1 = petrol:EtOAc) to yield ethyl 3-(4-methylthian-4-yl)-4-nitrobutanoate (**(±)-29**) (1.0 g, 43%). ^{1}H NMR ($CDCl_3$): δ 4.56 (dd, *J* = 12.8, 4.4 Hz, 1H), 4.35 (dd, *J* = 13.2, 7.6 Hz, 1H), 4.13 (q, *J* = 7.2 Hz, 2H), 3.67–3.77 (m, 1H), 2.78–2.68 (m, 3H), 2.61–2.53 (m, 2H), 2.30 (dd, *J* = 16.4, 8.4 Hz, 1H), 1.64–1.73 (m, 4H), 1.19–1.28 (m, 3H), 0.89 (s, 3H). Purity >90%.

4-(4-Methylthian-4-yl)pyrrolidin-2-one ((±)-30). A mixture of ethyl 3-(4-methylthian-4-yl)-4-nitrobutanoate (**(±)-29**) (216 mg, 0.79 mmol) in MeOH (16 mL) was cooled in an ice/water/salt bath and then $NiCl_2.6H_2O$ (205 mg, 0.86 mmol) was added. $NaBH_4$ (89 mg, 2.4 mmol) was carefully added in portions. The reaction was stirred for a further 1.5 hours with cooling and was then allowed to warm to ambient temperature. The reaction was quenched with 2M HCl and stirred for a further 1 hour. MeOH was removed *in vacuo* and the product was extracted with EtOAc (x3). The combined organic layers were washed with water and then brine. The organic layer was dried over $MgSO_4$, filtered and evaporated *in vacuo*. The product was purified by flash chromatography (gradient elution with MeOH/EtOAc) to yield

4-(4-methylthian-4-yl)pyrrolidin-2-one (**(±)-30**) as a colourless solid (102 mg, 65%). ^{1}H NMR ($CDCl_3$): δ 6.50 (br s, 1H), 3.32 (t, *J* = 9.1 Hz, 1H), 3.23 (t, *J* = 9.1 Hz, 1H), 2.83–2.70 (m, 2H), 2.54–2.43 (m, 3H), 2.21 (d, *J* = 9.7 Hz, 2H), 1.66–1.57 (m, 4H), 0.91 (s, 3H). ^{13}C NMR ($CDCl_3$): δ 177.9, 44.5, 42.4, 36.5, 35.9, 33.2, 30.8, 23.5, 23.4, 19.3. Purity >95%. HRMS (ESI-QTOF): *m/z* $[M+H]^+$ calculated for $C_{10}H_{17}NOS$ is 200.1104; Found 200.1105 (Δ = 0.68 ppm).

ASSOCIATED CONTENT

Supporting Information

Supporting Information contains biophysical assay protocols, supplementary tables, crystallographic details, in vitro assay details, PK details, synthetic schemes, experimental procedures and characterization of organic molecules.

Accession codes

Coordinates for the Lp-PLA_2 complexes with compounds **2–5**, **13, (*S*)-15, (*R*)-15, (±)-18** and **(*S*)-23** have been deposited in the Protein Data Bank (PDB) under accession codes: 5JAN (**2**), 5JAH (**3**), 5LZ2 (**4**), 5LYY (**5**), 5LZ4 (**13**), 5LZ5 (**(*S*)-15**), 5LZ7 (**(*R*)-15**), 5LZ8 (**(±)-18**) and 5LZ9 (**(*S*)-23**). Authors will release the atomic coordinates in experimental data upon article publication.

AUTHOR INFORMATION

Corresponding Authors

*Alison J.-A. Woolford. Tel: +44(0)1223 226283. Alison.Woolford@astx.com.

*Vipulkumar K. Patel. Tel: +44(0)1438 551281. Vipul.K.Patel@GSK.com.

Author Contributions

[#]A. J.-A. W. and P. J. D. contributed equally to this work.

ACKNOWLEDGMENTS

We would like to express our appreciation to Shenaz Bunally, Anne Cleasby, Marie-Hélène Fouchet, David Rees, Jeff Yon, Musundi B Wabuyele and Stuart Whibley for providing their support during the project, and our thanks to Ben Cons and Jeff St Denis for useful comments on the manuscript.

ABBREVIATIONS USED

HAC, heavy atom count; ITC, isothermal titration calorimetry; %I, percent inhibition of signal relative to solvent-only control; MW, molecular weight in g mol^{-1}; petrol, Petroleum ether; SBDD, structure-based drug design.

REFERENCES

1. (a) Six, D. A.; Dennis, E. A., The expanding superfamily of phospholipase A(2) enzymes: classification and characterization. *Biochim. Biophys. Acta* **2000**, *1488*, 1–19; (b) Schaloske, R. H.; Dennis, E. A., The phospholipase A2 superfamily and its group numbering system. *Biochim. Biophys. Acta* **2006**, *1761*, 1246–1259.

2. Stafforini, D. M.; McIntyre, T. M.; Carter, M. E.; Prescott, S. M., Human plasma platelet-activating factor acetylhydrolase. Association with lipoprotein particles and role in the degradation of platelet-activating factor. *J. Biol. Chem*. **1987**, *262*, 4215–4222.

3. (a) Stremler, K. E.; Stafforini, D. M.; Prescott, S. M.; Zimmerman, G. A.; McIntyre, T. M., An oxidized derivative of phosphatidylcholine is a substrate for the platelet-activating factor acetylhydrolase from human plasma. *J. Biol. Chem*. **1989**, *264*, 5331–5334; (b)

Stremler, K. E.; Stafforini, D. M.; Prescott, S. M.; McIntyre, T. M., Human plasma platelet-activating factor acetylhydrolase. Oxidatively fragmented phospholipids as substrates. *J. Biol. Chem*. **1991**, *266*, 11095–11103.

4. MacPhee, C. H.; Moores, K. E.; Boyd, H. F.; Dhanak, D.; Ife, R. J.; Leach, C. A.; Leake, D. S.; Milliner, K. J.; Patterson, R. A.; Suckling, K. E.; Tew, D. G.; Hickey, D. M., Lipoprotein-associated phospholipase A2, platelet-activating factor acetylhydrolase, generates two bioactive products during the oxidation of low-density lipoprotein: use of a novel inhibitor. *Biochem. J.* **1999**, *338 (Pt 2)*, 479–487.

5. Thompson, A.; Gao, P.; Orfei, L.; Watson, S.; Di Angelantonio, E.; Kaptoge, S.; Ballantyne, C.; Cannon, C. P.; Criqui, M.; Cushman, M.; Hofman, A.; Packard, C.; Thompson, S. G.; Collins, R.; Danesh, J., Lipoprotein-associated phospholipase A(2) and risk of coronary disease, stroke, and mortality: collaborative analysis of 32 prospective studies. *Lancet* **2010**, *375*, 1536–1544.

6. Fitzpatrick, A. L.; Irizarry, M. C.; Cushman, M.; Jenny, N. S.; Chi, G. C.; Koro, C., Lipoprotein-associated phospholipase A2 and risk of dementia in the Cardiovascular Health Study. *Atherosclerosis* **2014**, *235*, 384–391.

7. Staurenghi, G.; Ye, L.; Magee, M. H.; Danis, R. P.; Wurzelmann, J.; Adamson, P.; McLaughlin, M. M., Darapladib, a lipoprotein-associated phospholipase A2 inhibitor, in diabetic macular edema: a 3-month placebo-controlled study. *Ophthalmology* **2015**, *122*, 990–996.

8. (a) Vainio, P.; Gupta, S.; Ketola, K.; Mirtti, T.; Mpindi, J. P.; Kohonen, P.; Fey, V.; Perala, M.; Smit, F.; Verhaegh, G.; Schalken, J.; Alanen, K. A.; Kallioniemi, O.; Iljin, K., Arachidonic acid pathway members PLA2G7, HPGD, EPHX2, and CYP4F8 identified as putative novel therapeutic targets in prostate cancer. *Am. J. Pathol.* **2011**, *178*, 525–536; (b) Vainio, P.; Lehtinen, L.; Mirtti, T.; Hilvo, M.; Seppanen-Laakso, T.; Virtanen, J.; Sankila, A.;

Nordling, S.; Lundin, J.; Rannikko, A.; Oresic, M.; Kallioniemi, O.; Iljin, K., Phospholipase PLA2G7, associated with aggressive prostate cancer, promotes prostate cancer cell migration and invasion and is inhibited by statins. *Oncotarget* **2011**, *2*, 1176–1190; (c) Bertilsson, H.; Tessem, M. B.; Flatberg, A.; Viset, T.; Gribbestad, I.; Angelsen, A.; Halgunset, J., Changes in gene transcription underlying the aberrant citrate and choline metabolism in human prostate cancer samples. *Clin. Cancer Res.* **2012**, *18*, 3261–3269.

9. (a) Serruys, P. W.; Garcia-Garcia, H. M.; Buszman, P.; Erne, P.; Verheye, S.; Aschermann, M.; Duckers, H.; Bleie, O.; Dudek, D.; Botker, H. E.; von Birgelen, C.; D'Amico, D.; Hutchinson, T.; Zambanini, A.; Mastik, F.; van Es, G. A.; van der Steen, A. F.; Vince, D. G.; Ganz, P.; Hamm, C. W.; Wijns, W.; Zalewski, A.; Integrated, B.; Imaging Study, I., Effects of the direct lipoprotein-associated phospholipase A(2) inhibitor darapladib on human coronary atherosclerotic plaque. *Circulation* **2008**, *118*, 1172–1182; (b) Stability Investigators: White, H. D.; Held, C.; Stewart, R.; Tarka, E.; Brown, R.; Davies, R. Y.; Budaj, A.; Harrington, R. A.; Steg, P. G.; Ardissino, D.; Armstrong, P. W.; Avezum, A.; Aylward, P. E.; Bryce, A.; Chen, H.; Chen, M. F.; Corbalan, R.; Dalby, A. J.; Danchin, N.; De Winter, R. J.; Denchev, S.; Diaz, R.; Elisaf, M.; Flather, M. D.; Goudev, A. R.; Granger, C. B.; Grinfeld, L.; Hochman, J. S.; Husted, S.; Kim, H. S.; Koenig, W.; Linhart, A.; Lonn, E.; Lopez-Sendon, J.; Manolis, A. J.; Mohler, E. R., 3rd; Nicolau, J. C.; Pais, P.; Parkhomenko, A.; Pedersen, T. R.; Pella, D.; Ramos-Corrales, M. A.; Ruda, M.; Sereg, M.; Siddique, S.; Sinnaeve, P.; Smith, P.; Sritara, P.; Swart, H. P.; Sy, R. G.; Teramoto, T.; Tse, H. F.; Watson, D.; Weaver, W. D.; Weiss, R.; Viigimaa, M.; Vinereanu, D.; Zhu, J.; Cannon, C. P.; Wallentin, L., Darapladib for preventing ischemic events in stable coronary heart disease. *N. Engl. J. Med.* **2014**, *370*, 1702–1711.

10. Maher-Edwards, G.; De'Ath, J.; Barnett, C.; Lavrov, A.; Lockhart, A., A 24-week study to evaluate the effect of rilapladib on cognition and cerebrospinal fluid biomarkers of

Alzheimer's disease. *Alzheimer's & Dementia: Translational Research & Clinical Interventions* **2015**, *1*, 131–140.

11. Recombinant human Lp-PLA_2 Thio-PAF assay. This is the primary Lp-PLA_2 bioassay that was employed to measure inhibition in of Lp-PLA_2. It is a fluorescence intensity assay using Thio-Paf. See Supporting Information.

12. Recombinant human Lp-PLA_2 human plasma Thio-PAF assay. It is a secondary assay (also using Thio-Paf) that measures the inhibition of Lp-PLA_2 in whole human plasma. This assay functions to assess non-specific binding events of inhibitors in plasma and approximates the physiological environment of the enzyme. See Supporting Information.

13. Shaddinger, B. C.; Xu, Y.; Roger, J. H.; Macphee, C. H.; Handel, M.; Baidoo, C. A.; Magee, M.; Lepore, J. J.; Sprecher, D. L., Platelet aggregation unchanged by lipoprotein-associated phospholipase A(2) inhibition: results from an in vitro study and two randomized phase I trials. *PloS One* **2014**, e83094.

14. (a) Chen, X.; Xu, W.; Wang, K.; Mo, M.; Zhang, W.; Du, L.; Yuan, X.; Xu, Y.; Wang, Y.; Shen, J., Discovery of a novel series of imidazo[1,2-a]pyrimidine derivatives as potent and orally bioavailable lipoprotein-associated phospholipase A2 inhibitors. *J. Med. Chem.* **2015**, *58*, 8529–8541; (b) Nagano, J. M. G.; Hsu, K.-L.; Whitby, L. R.; Niphakis, M. J.; Speers, A. E.; Brown, S. J.; Spicer, T.; Fernandez-Vega, V.; Ferguson, J.; Hodder, P.; Srinivasan, P.; Gonzalez, T. D.; Rosen, H.; Bahnson, B. J.; Cravatt, B. F., Selective inhibitors and tailored activity probes for lipoprotein-associated phospholipase A_2. *Bioorg. Med. Chem. Lett.* **2013**, *23*, 839–843; (c) Tew, D. G.; Boyd, H. F.; Ashman, S.; Theobald, C.; Leach, C. A., Mechanism of inhibition of LDL phospholipase A2 by monocyclic-beta-lactams. Burst kinetics and the effect of stereochemistry. *Biochemistry* **1998**, *37*, 10087–10093; (d) Jeong, T. S.; Kim, M. J.; Yu, H.; Kim, K. S.; Choi, J. K.; Kim, S. S.; Lee, W. S., (*E*)-Phenyl- and -heteroaryl-substituted *O*-benzoyl-(or acyl)oximes as lipoprotein-associated phospholipase A2

inhibitors. *Bioorg. Med. Chem. Lett.* **2005**, *15*, 1525–1527; (e) Jeong, H. J.; Park, Y. D.; Park, H. Y.; Jeong, I. Y.; Jeong, T. S.; Lee, W. S., Potent inhibitors of lipoprotein-associated phospholipase A(2): benzaldehyde *O*-heterocycle-4-carbonyloxime. *Bioorg. Med. Chem. Lett.* **2006**, *16*, 5576–5579; (f) Lin, E. C.; Hu, Y.; Amantea, C. M.; Pham, L. M.; Cajica, J.; Okerberg, E.; Brown, H. E.; Fraser, A.; Du, L.; Kohno, Y.; Ishiyama, J.; Kozarich, J. W.; Shreder, K. R., Amides of xanthurenic acid as zinc-dependent inhibitors of Lp-PLA(2). *Bioorg. Med. Chem. Lett.* **2012**, *22*, 868–871; (g) Hu, Y.; Lin, E. C.; Pham, L. M.; Cajica, J.; Amantea, C. M.; Okerberg, E.; Brown, H. E.; Fraser, A.; Du, L.; Kohno, Y.; Ishiyama, J.; Kozarich, J. W.; Shreder, K. R., Amides of 4-hydroxy-8-methanesulfonylamino-quinoline-2-carboxylic acid as zinc-dependent inhibitors of Lp-PLA(2). *Bioorg. Med. Chem. Lett.* **2013**, *23*, 1553–1556; (h) Chen, X.; Wang, K.; Xu, W.; Ma, Q.; Chen, M.; Du, L.; Mo, M.; Wang, Y.; Shen, J., Discovery of potent and orally active lipoprotein-associated phospholipase A2 (Lp-PLA_2) inhibitors as a potential therapy for diabetic macular edema. *J. Med. Chem.* **2016**, *59*, 2674–2687.

15. Samanta, U.; Bahnson, B. J., Crystal structure of human plasma platelet-activating factor acetylhydrolase: structural implication to lipoprotein binding and catalysis. *J. Biol. Chem.* **2008**, *283*, 31617–31624.

16. (a) Woolford, A. J.-A.; Pero, J. E.; Aravapalli, S.; Berdini, V.; Coyle, J. E.; Day, P. J.; Dodson, A. M.; Grondin, P.; Holding, F. P.; Lee, L. Y.; Li, P.; Manas, E. S.; Marino, J., Jr.; Martin, A. C.; McCleland, B. W.; McMenamin, R. L.; Murray, C. W.; Neipp, C. E.; Page, L. W.; Patel, V. K.; Potvain, F.; Rich, S.; Rivero, R. A.; Smith, K.; Somers, D. O.; Trottet, L.; Velagaleti, R.; Williams, G.; Xie, R., Exploitation of a novel binding pocket in human lipoprotein-associated phospholipase A2 (Lp-PLA_2) discovered through X-ray fragment screening. *J. Med. Chem.* **2016**, *59*, 5356–5367; (b) Liu, Q.; Chen, X.; Chen, W.; Yuan, X.; Su, H.; Shen, J.; Xu, Y., Structural and thermodynamic characterization of protein-ligand

interactions formed between lipoprotein-associated phospholipase A2 and inhibitors. *J. Med. Chem.* **2016**, *59*, 5115–5120.

17. Rotella, D. P., SB-480848. GlaxoSmithKline. *Curr. Opin. Invest. Drugs* **2004**, *5*, 348–351.

18. CLOGP v4.93, Daylight Chemical Information Systems, Inc. http://www.daylight.com/dayhtml/doc/clogp/ (accessed 26th October 2016).

19. (a) Lipinski, C. A. L., F.; Dominy, B. W.; Feeney, P. J., Experimental and computational approaches to estimate solubility and permeability in drug discovery and development settings. *Adv. Drug Delivery Rev.* **1997**, *23*, 3–25; (b) Wenlock, M. C.; Austin, R. P.; Barton, P.; Davis, A. M.; Leeson, P. D., A comparison of physiochemical property profiles of development and marketed oral drugs. *J. Med. Chem.* **2003**, *46*, 1250–1256.

20. Smith, D. A.; Di, L.; Kerns, E. H., The effect of plasma protein binding on in vivo efficacy: misconceptions in drug discovery. *Nat. Rev. Drug Discovery* **2010**, *9*, 929–939.

21. Recombinant human Lp-PLA_2 PED6 assay using a PED6 fluorogenic substrate (employed for the weaker inhibitors). See Supporting Information.

22. Jones, G.; Willett, P.; Glen, R. C.; Leach, A. R.; Taylor, R., Development and validation of a genetic algorithm for flexible docking. *J. Mol. Biol.* **1997**, *267*, 727–748.

23. Ligand efficiency (LE) = $-\Delta G/HAC \approx -RT \ln(IC_{50})/HAC$ (units = kcal mol^{-1} per heavy atom). Hopkins, A. L.; Groom, C. R.; Alex, A., Ligand efficiency: a useful metric for lead selection. *Drug Discovery Today* **2004**, *9*, 430–431.

24. Group efficiency (GE) = $-\Delta\Delta G/\Delta HAC$ (units = kcal mol^{-1} per non-hydrogen atom). Verdonk, M. L.; Rees, D. C., Group efficiency: a guideline for hits-to-leads chemistry. *ChemMedChem* **2008**, *3*, 1179–1180.

Table of Contents graphic.

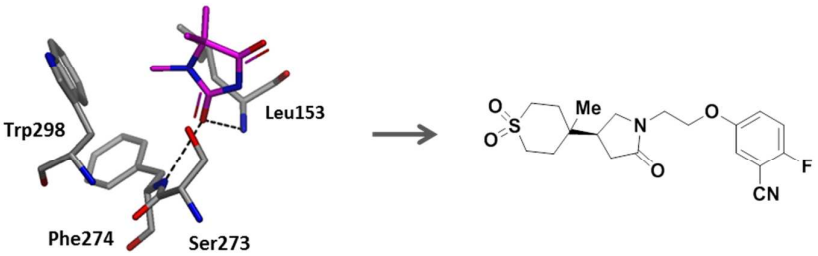

Starting fragment hit
IC_{50} >1mM

Lp-PLA_2 in whole human plasma assay: IC_{50} = 32 nM